Production of electroweak gauge bosons in off-shell gluon-gluon fusion

S. P. Baranov,[1] A. V. Lipatov,[2,*] and N. P. Zotov[2]

[1]*P.N. Lebedev Physics Institute, 119991 Moscow, Russia*
[2]*D.V. Skobeltsyn Institute of Nuclear Physics, M.V. Lomonosov Moscow State University, 119991 Moscow, Russia*
(Received 9 June 2008; published 29 July 2008)

We study the production of electroweak gauge bosons at high energies in the framework of k_T-factorization QCD approach. The amplitude for production of a single $W^\pm$ or Z^0 boson associated with quark pair in the fusion of two off-shell gluons is calculated. Contributions from the valence quarks are calculated using the quark-gluon interaction and quark-antiquark annihilation QCD subprocesses. The total and differential cross sections (as a function of the transverse momentum and rapidity) are presented and the ratio of cross sections for $W^\pm$ and Z^0 boson production is investigated. The conservative error analysis is performed. In the numerical calculations two different sets of unintegrated gluon distributions in the proton are used: the one obtained from the Ciafaloni-Catani-Fiorani-Marchesini evolution equation and the other from the Kimber-Martin-Ryskin prescription. Theoretical results are compared with experimental data taken by the D0 and CDF collaborations at the Tevatron. We demonstrate the importance of the quark component in parton evolution in description of the experimental data. This component is very significant also at the LHC energies.

PACS numbers: 12.38.Bx, 12.15.Ji

I. INTRODUCTION

The theoretical and experimental studying of the vector ($W^\pm$ and Z^0) boson production at high energies provides information about the nature of both the underlying electroweak interaction and the effects of quantum chromodynamics (QCD). In many respects these processes have become one of the most important ''standard candles'' in experimental high-energy physics [1–9]. At the Tevatron, measurements of $W^\pm$ and Z^0 inclusive cross sections are routinely used to validate detector and trigger performance and stability. Data from gauge boson production also provide bounds on parametrizations used to describe the nonperturbative regime of QCD processes. At the LHC, such measurements can serve as a useful tool to determine the integrated luminosity and can also be used to normalize measurements of other production cross sections (for example, the cross section of $W + n$-jets or diboson production). Additionally, the studying of inclusive vector boson production is the necessary starting point for investigations of Higgs or top quark production where many signatures can include these bosons.

At leading order (LO) of QCD, $W^\pm$ and Z^0 bosons are produced via quark-antiquark annihilation. Beyond the LO Born process, the vector boson can also be produced by $q + g$ interactions, so both the quark and gluon distribution functions of the proton play an important role. Theoretical calculations of the $W^\pm$ and Z^0 production cross sections have been carried out at next-to-leading order (NLO) and next-to-next-to-leading order (NNLO) [10–14] of QCD. The NLO cross section is ∼25% larger than the Born-level cross section, and the NNLO cross section is an additional

∼3% higher. However, these perturbative calculations are reliable at high p_T only since they diverge in the small $p_T \ll m$ region with terms proportional to $\ln m/p_T$ (appearing due to soft and collinear gluon emission). Therefore, the soft gluon resummation technique [15–19] should be used to make QCD predictions at low p_T. The traditional calculations combine fixed-order perturbation theory with analytic resummation and some matching criterion. The analytic resummation can be performed either in the transverse momentum space [20] or in the Fourier conjugate impact parameter space [21]. Differences between the two formalisms are discussed in [22].

An alternative description can be provided by the k_T-factorization approach of QCD [23,24]. This approach is based on the familiar Balitsky-Fadin-Kuraev-Lipatov (BFKL) [25] or Catani-Ciafaloni-Fiorani-Marchesini (CCFM) [26] gluon evolution equations and takes into account the large logarithmic terms proportional to $\ln 1/x$. This contrasts with the usual Dokshitzer-Gribov-Lipatov-Altarelli-Parisi (DGLAP) [27] strategy where only the large logarithmic terms proportional to $\ln \mu^2$ are taken into account. The basic dynamical quantity of the k_T-factorization approach is the unintegrated (i.e., $\mathbf{k}_T$-dependent) parton distribution $f_a(x, \mathbf{k}_T^2, \mu^2)$ which determines the probability to find a type a parton carrying the longitudinal momentum fraction x and the transverse momentum $\mathbf{k}_T$ at the probing scale μ^2. In this approach, since each incoming parton carries its own nonzero transverse momentum, the Born-level subprocess $q + \bar{q}' \to W^\pm/Z^0$ already generates the p_T distribution of the produced vector boson. Similar to DGLAP, to calculate the cross sections of any physical process the unintegrated parton density $f_a(x, \mathbf{k}_T^2, \mu^2)$ has to be convoluted [23,24] with the relevant partonic cross section which has to be taken

*lipatov@theory.sinp.msu.ru

off-mass shell ($\mathbf{k}_T$-dependent). The soft gluon resummation formulas are the result of the approximate treatment of the solutions of the CCFM evolution equation [28]. Other important properties of the k_T-factorization formalism are the additional contribution to the cross sections due to the integration over the $\mathbf{k}_T^2$ region above μ^2 and the broadening of the transverse momentum distributions due to extra transverse momentum of the colliding partons.[1]

The k_T-factorization formalism has been already applied [30] to calculate transverse momentum distribution of the inclusive $W^\pm$ and Z^0 production at Tevatron. The calculations [30] were based on the usual (on-mass shell) matrix elements of the quark-antiquark annihilation subprocess $q + \bar{q}' \rightarrow W^\pm/Z^0$ which embedded in precise off-shell kinematics. However, an important component of the calculations [30] is the unintegrated quark distribution in a proton. At present these distributions are only available in the framework of the Kimber-Martin-Ryskin (KMR) approach [31] since there are some theoretical difficulties in obtaining the quark densities immediately from CCFM or BFKL equations[2] (see, for example, reviews [29] for more details). As a result the dependence of the calculated cross sections on the noncollinear evolution scheme has not been investigated. This dependence in general can be significant and it is a special subject of study in the k_T-factorization formalism. Therefore in the present paper we will try a different and more systematic way. Instead of using the unintegrated quark distributions and the corresponding quark-antiquark annihilation cross section we calculate the off-shell matrix element of the $g^* + g^* \rightarrow W^\pm/Z^0 + q + \bar{q}'$ subprocess and then operate in terms of the unintegrated gluon densities only. In this scenario, at the price of considering the $2 \rightarrow 3$ rather than $2 \rightarrow 1$ matrix elements, the problem of unknown unintegrated quark distributions will reduce to the problem of gluon distributions. However, since the gluons are only responsible for the appearance of the sea but not valence quarks, the contribution from the valence quarks should be calculated separately. Having in mind that the valence quarks are only important at large x, where the traditional DGLAP evolution is accurate and reliable, this contribution can be taken into account within the usual collinear scheme based on the $q + g^* \rightarrow W^\pm/Z^0 + q'$ and $q + \bar{q}' \rightarrow W^\pm/Z^0$ matrix elements convoluted with the on-shell valence quark and/or off-shell gluon densities.[3] Thus, the proposed way enables us with making comparisons between the different parton evolution schemes and parametrizations of parton densities.[4]

We should mention, of course, that this idea can only work well if the sea quarks appear from the last step of the gluon evolution—then we can absorb this last step of the gluon ladder into a hard matrix element. However, this method does not apply to the quarks coming from the earlier steps of the evolution (i.e., from the second-to-last, third-to-last, and other gluon splittings). But it is not evident in advance, whether the last gluon splitting dominates or not. The goal of our study is to clarify this point.

The outline of our paper is following. In Sec. II we recall shortly the basic formulas of the k_T-factorization approach with a brief review of calculation steps and the unintegrated parton densities used. We will concentrate mainly on the $g^* + g^* \rightarrow W^\pm/Z^0 + q + \bar{q}'$ subprocess. The evaluation of $q + g^* \rightarrow W^\pm/Z^0 + q'$ and $q + \bar{q}' \rightarrow W^\pm/Z^0$ contributions is straightforward and, for the reader's convenience, we only collect the main relevant formulas in the appendix. In Sec. III we present the numerical results of our calculations. The central point is discussing the role of each contribution mentioned above to the cross section. Special attention is put on the transverse momentum distributions of the $W^\pm$ and Z^0 boson measured by the D0 [5,8,9] and CDF [4] collaborations. Section IV contains our conclusions.

II. THEORETICAL FRAMEWORK

As the off-shell gluon-gluon fusion $g^* + g^* \rightarrow W^\pm/Z^0 + q + \bar{q}'$ is calculated for the first time in the literature, we find it reasonable to explain it in more detail.

A. Kinematics

We start from the kinematics (see Fig. 1). Let $p^{(1)}$ and $p^{(2)}$ be the four-momenta of the incoming protons and p the four-momentum of the produced $W^\pm/Z^0$ boson. The initial off-shell gluons have the four-momenta k_1 and k_2 and the final quark q and antiquark $\bar{q}'$ have the four-momenta p_1 and p_2 and the masses m_1 and m_2, respec-
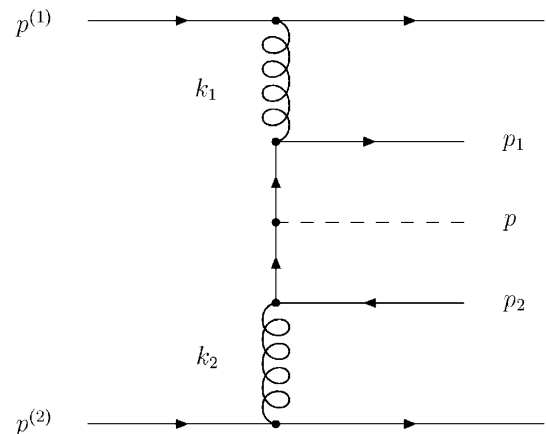

FIG. 1. Kinematics of the $g^* + g^* \rightarrow W^\pm/Z^0 + q + q'$ process.

---

[1] For an introduction to k_T-factorization, see, for example, review [29].

[2] Unintegrated quark density was considered recently in [32].

[3] To avoid the double counting we have not considered here the $q + \bar{q}' \rightarrow W^\pm/Z^0 + g$ subprocess.

[4] The similar scenario has been applied recently to the prompt photon hadroproduction at the Tevatron [33].

tively. In the $p\bar{p}$ center-of-mass frame we can write

$$p^{(1)} = \frac{\sqrt{s}}{2}(1, 0, 0, 1), \qquad p^{(2)} = \frac{\sqrt{s}}{2}(1, 0, 0, -1), \quad (1)$$

where $\sqrt{s}$ is the total energy of the process under consideration and we neglect the masses of the incoming protons. The initial gluon four-momenta in the high-energy limit can be written as

$$k_1 = x_1 p^{(1)} + k_{1T}, \qquad k_2 = x_2 p^{(2)} + k_{2T}, \quad (2)$$

where k_{1T} and k_{2T} are the transverse four-momenta. It is important that $\mathbf{k}_{1T}^2 = -k_{1T}^2 \neq 0$ and $\mathbf{k}_{2T}^2 = -k_{2T}^2 \neq 0$. From the conservation laws we can obtain the following relations:

$$\begin{aligned}\mathbf{k}_{1T} + \mathbf{k}_{2T} &= \mathbf{p}_{1T} + \mathbf{p}_{2T} + \mathbf{p}_T, \\ x_1\sqrt{s} &= m_{1T}e^{y_1} + m_{2T}e^{y_2} + m_T e^{y}, \\ x_2\sqrt{s} &= m_{1T}e^{-y_1} + m_{2T}e^{-y_2} + m_T e^{-y}, \end{aligned} \quad (3)$$

where p_T, m_T, and y are the transverse momentum, transverse mass, and center-of-mass rapidity of the produced $W^\pm/Z^0$ boson, p_{1T} and p_{2T} are the transverse momenta of final quark q and antiquark $\bar{q}'$, y_1, y_2, m_{1T}, and m_{2T} are their rapidities and transverse masses, i.e. $m_{iT}^2 = m_i^2 + \mathbf{p}_{iT}^2$.

B. Off-shell amplitude of the $g^* + g^* \rightarrow W^\pm/Z^0 + q + \bar{q}'$ subprocess

There are eight Feynman diagrams (see Fig. 2) which describe the partonic subprocess $g^* + g^* \rightarrow W^\pm/Z^0 + q + \bar{q}'$ at $\alpha\alpha_s^2$ order. Let ϵ_1, ϵ_2, and ϵ be the initial gluon and produced gauge boson polarization vectors, respectively, and a and b the eightfold color indices of the off-shell gluons. Then the relevant matrix element can be presented as follows:

$$\begin{aligned}\mathcal{M}_1 = g^2 \bar{u}(p_1) t^a \gamma^\mu \epsilon_\mu \frac{\hat{p}_1 - \hat{k}_1 + m_1}{m_1^2 - (p_1 - k_1)^2} T_{W,Z}^\lambda \epsilon_\lambda \\ \times \frac{\hat{k}_2 - \hat{p}_2 + m_2}{m_2^2 - (k_2 - p_2)^2} t^b \gamma^\nu \epsilon_\nu u(p_2), \end{aligned} \quad (4)$$

$$\begin{aligned}\mathcal{M}_2 = g^2 \bar{u}(p_1) t^b \gamma^\nu \epsilon_\nu \frac{\hat{p}_1 - \hat{k}_2 + m_1}{m_1^2 - (p_1 - k_2)^2} T_{W,Z}^\lambda \epsilon_\lambda \\ \times \frac{\hat{k}_1 - \hat{p}_2 + m_2}{m_2^2 - (k_1 - p_2)^2} t^a \gamma^\mu \epsilon_\mu u(p_2), \end{aligned} \quad (5)$$

$$\begin{aligned}\mathcal{M}_3 = g^2 \bar{u}(p_1) t^a \gamma^\mu \epsilon_\mu \frac{\hat{p}_1 - \hat{k}_1 + m_1}{m_1^2 - (p_1 - k_1)^2} t^b \gamma^\nu \epsilon_\nu \\ \times \frac{-\hat{p}_2 - \hat{p} + m_1}{m_1^2 - (-p_2 - p)^2} T_{W,Z}^\lambda \epsilon_\lambda u(p_2), \end{aligned} \quad (6)$$
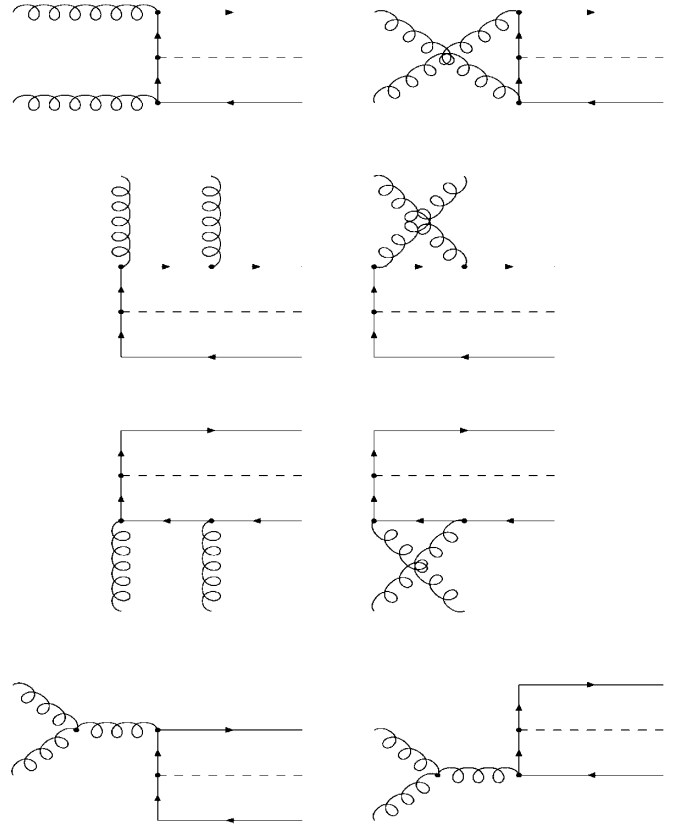

FIG. 2. Feynman diagrams which describe the partonic subprocess $g^* + g^* \rightarrow W^\pm/Z^0 + q + q'$ at the leading order in α_s and α.

$$\begin{aligned}\mathcal{M}_4 = g^2 \bar{u}(p_1) t^b \gamma^\nu \epsilon_\nu \frac{\hat{p}_1 - \hat{k}_2 + m_1}{m_1^2 - (p_1 - k_2)^2} t^a \gamma^\mu \epsilon_\mu \\ \times \frac{-\hat{p}_2 - \hat{p} + m_1}{m_1^2 - (-p_2 - p)^2} T_{W,Z}^\lambda \epsilon_\lambda u(p_2), \end{aligned} \quad (7)$$

$$\begin{aligned}\mathcal{M}_5 = g^2 \bar{u}(p_1) T_{W,Z}^\lambda \epsilon_\lambda \frac{\hat{p}_1 + \hat{p} + m_2}{m_2^2 - (p_1 + p)^2} t^b \gamma^\nu \epsilon_\nu \\ \times \frac{\hat{k}_1 - \hat{p}_2 + m_2}{m_2^2 - (k_1 - p_2)^2} t^a \gamma^\mu \epsilon_\mu u(p_2), \end{aligned} \quad (8)$$

$$\begin{aligned}\mathcal{M}_6 = g^2 \bar{u}(p_1) T_{W,Z}^\lambda \epsilon_\lambda \frac{\hat{p}_1 + \hat{p} + m_2}{m_2^2 - (p_1 + p)^2} t^a \gamma^\mu \epsilon_\mu \\ \times \frac{\hat{k}_2 - \hat{p}_2 + m_2}{m_2^2 - (k_2 - p_2)^2} t^b \gamma^\nu \epsilon_\nu u(p_2), \end{aligned} \quad (9)$$

$$\begin{aligned}\mathcal{M}_7 = g^2 \bar{u}(p_1) \gamma^\rho C^{\mu\nu\rho}(k_1, k_2, -k_1 - k_2) \\ \times \frac{\epsilon_\mu \epsilon_\nu}{(k_1 + k_2)^2} f^{abc} t^c \\ \times \frac{-\hat{p}_2 - \hat{p} + m_1}{m_1^2 - (-p_2 - p)^2} T_{W,Z}^\lambda \epsilon_\lambda u(p_2), \end{aligned} \quad (10)$$

$$\mathcal{M}_8 = g^2 \bar{u}(p_1) T^\lambda_{W,Z} \epsilon_\lambda \frac{\hat{p}_1 + \hat{p} + m_2}{m_2^2 - (p_1 + p)^2}$$

$$\times \gamma^\rho C^{\mu\nu\rho}(k_1, k_2, -k_1 - k_2)$$

$$\times \frac{\epsilon_\mu \epsilon_\nu}{(k_1 + k_2)^2} f^{abc} t^c u(p_2). \qquad (11)$$

In the above expressions $C^{\mu\nu\rho}(k, p, q)$ and $T^\lambda_{W,Z}$ are related to the standard QCD three-gluon coupling and the $W^\pm/Z^0$-fermion vertexes:

$$C^{\mu\nu\rho}(k, p, q) = g^{\mu\nu}(p - k)^\rho + g^{\nu\rho}(q - p)^\mu$$

$$+ g^{\rho\mu}(k - q)^\nu, \qquad (12)$$

$$T^\lambda_W = \frac{e}{2\sqrt{2}\sin\theta_W} \gamma^\lambda (1 - \gamma^5) V_{qq'}, \qquad (13)$$

$$T^\lambda_Z = \frac{e}{\sin2\theta_W} \gamma^\lambda [I_3^{(q)}(1 - \gamma^5) - 2e_q \sin^2\theta_W], \qquad (14)$$

where $I_3^{(q)}$ and e_q are the weak isospin and the fractional electric charge (in the positron charge e units) of the final-state quark q, θ_W is the Weinberg mixing angle, and $V_{qq'}$ is the Cabibbo-Kobayashi-Maskawa (CKM) matrix element. Of course, in the case of Z^0 production m_1 equals m_2. The summation on the $W^\pm/Z^0$ polarization is carried out by the covariant formula

$$\sum \epsilon^\mu(p)\epsilon^{*\nu}(p) = -g^{\mu\nu} + \frac{p^\mu p^\nu}{m^2}. \qquad (15)$$

In the case of the initial off-shell gluon we use the BFKL prescription [23,24]:

$$\sum \epsilon^\mu(k_i)\epsilon^{*\nu}(k_i) = \frac{k_{iT}^\mu k_{iT}^\nu}{\mathbf{k}_{iT}^2}. \qquad (16)$$

This formula converges to the usual expression $\sum \epsilon^\mu \epsilon^{*\nu} = -g^{\mu\nu}$ after azimuthal angle averaging in the $k_T \to 0$ limit. The evaluation of the traces in (4)–(11) was done using the algebraic manipulation system FORM [34]. We would like to mention here that the usual method of squaring of (4)–(11) results in enormously long output. This technical problem was solved by applying the method of orthogonal amplitudes [35].

The gauge invariance of the matrix element is a subject of special attention in the k_T-factorization approach. Strictly speaking, the diagrams shown in Fig. 2 are insufficient and have to be accompanied with the graphs involving direct gluon exchange between the protons (these protons are not shown in Fig. 2). These graphs are necessary to maintain the gauge invariance. However, they violate the factorization since they cannot be represented as a convolution of the gluon-gluon fusion matrix element with unintegrated gluon density. The solution pointed out in [24] refers to the fact that, within the particular gauge (16), the contribution from these unfactorizable diagrams vanish, and one has to only take into account the graphs depicted in Fig. 2. We have successfully tested the gauge invariance of the matrix element (4)–(11) numerically.[5]

C. Cross section for the inclusive $W^\pm/Z^0$ production

According to the k_T-factorization theorem, the inclusive $W^\pm/Z^0$ production cross section via two off-shell gluon fusion can be written as a convolution

$$\sigma(p + \bar{p} \to W^\pm/Z^0 + X) = \sum_q \int \frac{dx_1}{x_1} f_g(x_1, \mathbf{k}_{1T}^2, \mu^2) d\mathbf{k}_{1T}^2 \frac{d\phi_1}{2\pi} \times \int \frac{dx_2}{x_2} f_g(x_2, \mathbf{k}_{2T}^2, \mu^2) d\mathbf{k}_{2T}^2 \frac{d\phi_2}{2\pi} d\hat{\sigma}(g^* + g^*$$

$$\to W^\pm/Z^0 + q + \bar{q}'), \qquad (17)$$

where $\hat{\sigma}(g^* + g^* \to W^\pm/Z^0 + q + \bar{q}')$ is the partonic cross section, $f_g(x, \mathbf{k}_T^2, \mu^2)$ is the unintegrated gluon distribution in a proton, and ϕ_1 and ϕ_2 are the azimuthal angles of the incoming gluons. The multiparticle phase space $\Pi d^3 p_i / 2E_i \delta^{(4)}(\sum p^{\text{in}} - \sum p^{\text{out}})$ is parametrized in terms of transverse momenta, rapidities, and azimuthal angles:

$$\frac{d^3 p_i}{2E_i} = \frac{\pi}{2} d\mathbf{p}_{iT}^2 dy_i \frac{d\phi_i}{2\pi}. \qquad (18)$$

Using the expressions (17) and (18) we obtain the master formula:

$$\sigma(p + \bar{p} \to W^\pm/Z^0 + X) = \sum_q \int \frac{1}{256\pi^3 (x_1 x_2 s)^2} |\bar{\mathcal{M}}(g^* + g^* \to W^\pm/Z^0 + q + \bar{q}')|^2$$

$$\times f_g(x_1, \mathbf{k}_{1T}^2, \mu^2) f_g(x_2, \mathbf{k}_{2T}^2, \mu^2) d\mathbf{k}_{1T}^2 d\mathbf{k}_{2T}^2 d\mathbf{p}_{1T}^2 \mathbf{p}_{2T}^2 dy dy_1 dy_2 \frac{d\phi_1}{2\pi} \frac{d\phi_2}{2\pi} \frac{d\psi_1}{2\pi} \frac{d\psi_2}{2\pi}, \qquad (19)$$

---

[5]At the preliminary stage of the work we have made a cross-check of the matrix elements which have been calculated independently by M. Deak and F. Schwennsen.

where $|\bar{\mathcal{M}}(g^* + g^* \to W^\pm/Z^0 + q + \bar{q}')|^2$ is the off-mass shell matrix element squared and averaged over initial gluon polarizations and colors, ψ_1 and ψ_2 are the azimuthal angles of the final-state quark and antiquark, respectively. We would like to point out again that $|\bar{\mathcal{M}}(g^* + g^* \to W^\pm/Z^0 + q + \bar{q}')|^2$ strongly depends on the nonzero transverse momenta $\mathbf{k}_{1T}^2$ and $\mathbf{k}_{2T}^2$. If we average the expression (19) over ϕ_1 and ϕ_2 and take the limit $\mathbf{k}_{1T}^2 \to 0$ and $\mathbf{k}_{2T}^2 \to 0$, then we recover the expression for the $W^\pm/Z^0$ production cross section in the collinear $\alpha\alpha_s^2$ approximation.

The multidimensional integration in (19) has been performed by means of the Monte Carlo technique, using the routine VEGAS [36]. The full C++ code is available from the authors upon request.

D. The KMR unintegrated parton distributions

In the present paper we have tried two different sets of unintegrated parton densities in a proton. The first of them is the Kimber-Martin-Ryskin set.

The KMR approach [31] is the formalism to construct parton distributions $f_a(x, \mathbf{k}_T^2, \mu^2)$ unintegrated over the parton transverse momenta $\mathbf{k}_T^2$ from the known conventional parton distributions $xa(x, \mu^2)$, where $a = g$ or $a = q$. This formalism is valid for a proton as well as a photon and can embody both DGLAP and BFKL contributions. It also accounts for the angular ordering which comes from coherence effects in gluon emission. The key observation here is that the μ dependence of the unintegrated parton distributions $f_a(x, \mathbf{k}_T^2, \mu^2)$ enters at the last step of the evolution, and therefore single scale evolution equations (pure DGLAP) can be used up to this step. In this approximation, the unintegrated quark and gluon distributions are given by the expressions [31]

$$
\begin{aligned}
f_q(x, \mathbf{k}_T^2, \mu^2) = {}& T_q(\mathbf{k}_T^2, \mu^2)\frac{\alpha_s(\mathbf{k}_T^2)}{2\pi} \\
& \times \int_x^1 dz \Bigg[P_{qq}(z)\frac{x}{z}q\Big(\frac{x}{z}, \mathbf{k}_T^2\Big)\Theta(\Delta - z) \\
& + P_{qg}(z)\frac{x}{z}g\Big(\frac{x}{z}, \mathbf{k}_T^2\Big) \Bigg],
\end{aligned}
\tag{20}
$$

$$
\begin{aligned}
f_g(x, \mathbf{k}_T^2, \mu^2) = {}& T_g(\mathbf{k}_T^2, \mu^2)\frac{\alpha_s(\mathbf{k}_T^2)}{2\pi} \\
& \times \int_x^1 dz \Bigg[\sum_q P_{gq}(z)\frac{x}{z}q\Big(\frac{x}{z}, \mathbf{k}_T^2\Big) \\
& + P_{gg}(z)\frac{x}{z}g\Big(\frac{x}{z}, \mathbf{k}_T^2\Big)\Theta(\Delta - z) \Bigg],
\end{aligned}
\tag{21}
$$

where $P_{ab}(z)$ are the usual unregulated leading-order DGLAP splitting functions, and $q(x, \mu^2)$ and $g(x, \mu^2)$ are the conventional quark and gluon densities.[6] The theta

---

[6]Numerically, we have used the standard GRV (LO) parametrizations [37].

functions which appear in (20) and (21) imply the angular-ordering constraint $\Delta = \mu/(\mu + |\mathbf{k}_T|)$ specifically to the last evolution step to regulate the soft gluon singularities. For other evolution steps, the strong ordering in transverse momentum within the DGLAP equations automatically ensures angular ordering. It is important that the parton distributions $f_a(x, \mathbf{k}_T^2, \mu^2)$ are extended now into the $\mathbf{k}_T^2 > \mu^2$ region. This fact is in clear contrast with the usual DGLAP evolution.[7]

The virtual (loop) contributions may be resummed to all orders by the quark and gluon Sudakov form factors

$$
\ln T_q(\mathbf{k}_T^2, \mu^2) = -\int_{\mathbf{k}_T^2}^{\mu^2} \frac{d\mathbf{p}_T^2}{\mathbf{p}_T^2}\frac{\alpha_s(\mathbf{p}_T^2)}{2\pi}\int_0^{z_{max}} dz P_{qq}(z),
\tag{22}
$$

$$
\begin{aligned}
\ln T_g(\mathbf{k}_T^2, \mu^2) = {}& -\int_{\mathbf{k}_T^2}^{\mu^2} \frac{d\mathbf{p}_T^2}{\mathbf{p}_T^2}\frac{\alpha_s(\mathbf{p}_T^2)}{2\pi}\Bigg[n_f\int_0^1 dz P_{qg}(z) \\
& + \int_{z_{min}}^{z_{max}} dz z P_{gg}(z) \Bigg],
\end{aligned}
\tag{23}
$$

where $z_{max} = 1 - z_{min} = \mu/(\mu + |\mathbf{p}_T|)$. The form factors $T_a(\mathbf{k}_T^2, \mu^2)$ give the probability of evolving from a scale $\mathbf{k}_T^2$ to a scale μ^2 without parton emission. In accordance with (22) and (23) $T_a(\mathbf{k}_T^2, \mu^2) = 1$ in the $\mathbf{k}_T^2 > \mu^2$ region.

Note that such definition of the $f_a(x, \mathbf{k}_T^2, \mu^2)$ is correct for $\mathbf{k}_T^2 > \mu_0^2$ only, where $\mu_0 \sim 1$ GeV is the minimum scale for which DGLAP evolution of the collinear parton densities is valid. Everywhere in our numerical calculations we set the starting scale μ_0 to equal $\mu_0 = 1$ GeV. Since the starting point of this derivation is the leading-order DGLAP equations, the unintegrated parton distributions must satisfy the normalization condition

$$
a(x, \mu^2) = \int_0^{\mu^2} f_a(x, \mathbf{k}_T^2, \mu^2) d\mathbf{k}_T^2.
\tag{24}
$$

This relation will be exactly satisfied if one defines [31]

$$
f_a(x, \mathbf{k}_T^2, \mu^2)|_{\mathbf{k}_T^2 < \mu_0^2} = a(x, \mu_0^2) T_a(\mu_0^2, \mu^2).
\tag{25}
$$

E. The CCFM unintegrated gluon distribution

The CCFM gluon density has been obtained [38] from the numerical solution of the CCFM equation. The function $f_g(x, \mathbf{k}_T^2, \mu^2)$ is determined by a convolution of the nonperturbative starting distribution $f_g^{(0)}(x)$ and the CCFM evolution kernel denoted by $\tilde{\mathcal{A}}(x, \mathbf{k}_T^2, \mu^2)$:

$$
f_g(x, \mathbf{k}_T^2, \mu^2) = \int\frac{dx'}{x'}f_g^{(0)}(x')\tilde{\mathcal{A}}\Big(\frac{x}{x'}, \mathbf{k}_T^2, \mu^2\Big).
\tag{26}
$$

---

[7]We would like to note that cutoff Δ can be taken $\Delta = |\mathbf{k}_T|/\mu$; also in [31]. In this case the unintegrated parton distributions given by (20) and (21) vanish for $\mathbf{k}_T^2 > \mu^2$ in accordance with the DGLAP strong ordering in $\mathbf{k}_T^2$.

In the perturbative evolution the gluon splitting function $P_{gg}(z)$ including nonsingular terms is applied, as it was described in [39]. The input parameters in $f_g^{(0)}(x)$ were fitted to reproduce the proton structure functions $F_2(x, Q^2)$. An acceptable fit to the measured F_2 values was obtained [38] with $\chi^2/ndf = 1.83$ using statistical and uncorrelated systematic uncertainties (compare to $\chi^2/ndf \sim 1.5$ in the collinear approach at NLO).

III. NUMERICAL RESULTS

We are now in a position to present our numerical results. First we describe the theoretical uncertainties of our consideration.

Besides the unintegrated parton distributions in a proton $f_q(x, \mathbf{k}_T^2, \mu^2)$, there are several parameters which determined the overall normalization factor of the calculated $W^\pm/Z^0$ cross sections: the quark masses m_1 and m_2 and the factorization and renormalization scales μ_F and μ_R (the first of them is related to the evolution of the parton distributions, the other is responsible for the strong coupling constant). In the numerical calculations the masses of light quarks were set to be equal to $m_u = 4.5$ MeV, $m_d = 8.5$ MeV, $m_s = 155$ MeV and the charmed quark mass was set to $m_c = 1.5$ GeV. We have checked that uncertainties which come from these quantities are negligible in comparison to the uncertainties connected with the scale and/or the unintegrated parton densities. As is often done, we choose the renormalization and factorization scales to be equal: $\mu_R = \mu_F = \mu = \xi m_T$ (transverse mass of the produced vector boson). In order to investigate the scale dependence of our results we vary the scale parameter ξ between $1/2$ and 2 about the default value $\xi = 1$. For completeness, we set $m_W = 80.403$ GeV, $m_Z = 91.1876$ GeV, $\sin^2\theta_W = 0.23122$ and use the LO formula for the strong coupling constant $\alpha_s(\mu^2)$ with $n_f = 4$ active quark flavors at $\Lambda_{\rm QCD} = 200$ MeV (so that $\alpha_s(M_Z^2) = 0.1232$). Note that we use a special choice $\Lambda_{\rm QCD} = 130$ MeV in the case of the CCFM gluon ($\alpha_s(M_Z^2) = 0.1187$), as was originally proposed in [38].

Before we proceed to the numerical results, we would like to comment on the effect of the higher order QCD contributions [30]. It is well known that the leading-order k_T-factorization approach naturally includes a large part of them.[8] It is corrections which are kinematic in nature arising from the real parton emission during the evolution cascade. Another part of high-order contributions comes from the logarithmic loop corrections which have already been included in the Sudakov form factors (22) and (23). However, there are also the nonlogarithmic loop corrections, arising, for example, from the gluon vertex corrections to Fig. 2. To take into account these contributions we will use the approach proposed in [30]. It was demon-

strated that the main part of the nonlogarithmic loop corrections can be absorbed in the so-called K-factor given by the expression

$$K(q + \bar{q}' \to W^\pm/Z^0) \simeq \exp\left[C_F \frac{\alpha_s(\mu^2)}{2\pi} \pi^2\right], \quad (27)$$

where the color factor $C_F = 4/3$. A particular choice $\mu^2 = \mathbf{p}_T^{4/3} m^{2/3}$ has been proposed [22,30] to eliminate subleading logarithmic terms. We choose this scale to evaluate the strong coupling constant $\alpha_s(\mu^2)$ in (27).

We begin the discussion by presenting a comparison between the different contributions to the $W^\pm/Z^0$ total cross section. The solid, dashed, and dotted histograms in Figs. 3–6 represent the $g^* + g^* \to W^\pm/Z^0 + q + \bar{q}'$, $q + q^* \to W^\pm/Z^0 + q'$, and $q + \bar{q}' \to W^\pm/Z^0$ contributions to the rapidity distributions of the gauge boson calculated at the Tevatron (Figs. 3 and 4) and LHC conditions (Figs. 5 and 6). It is important that in the last two subprocesses we take into account only the valence quarks within the usual collinear approximation. For illustration, we used here the KMR unintegrated gluon density. We found that the role of the gluon-gluon fusion subprocess is greatly increased at the LHC energy: it contributes only about 2% or 3% of the valence quark component at the Tevatron and more than 40% at the LHC. Moreover, in the last case it dominates
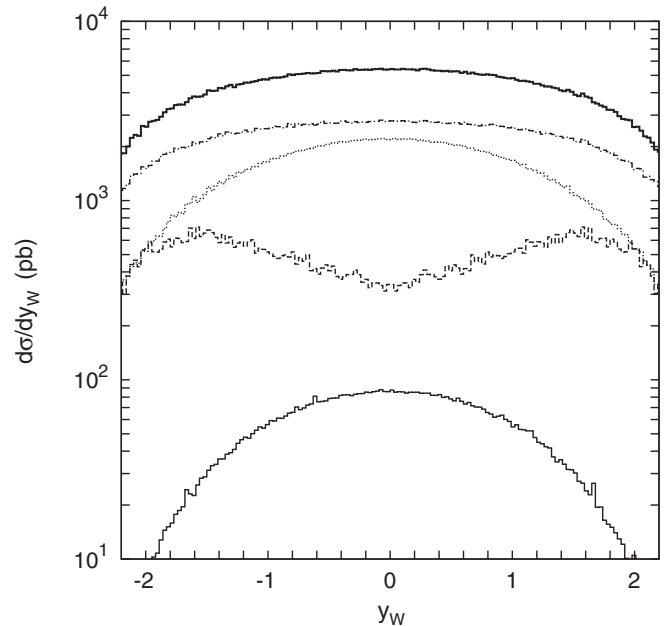

FIG. 3. Different contributions to the inclusive $W^\pm$ boson production at the Tevatron conditions. The solid, dashed, and dotted histograms correspond to the $g^* + g^* \to W^\pm + q + \bar{q}'$, $q + g^* \to W^\pm + q'$, and $q + \bar{q}' \to W^\pm$ subprocesses. In the last two cases only the valence quarks are taken into account. The dash-dotted histogram represents the contribution from the quarks coming from the earlier steps of the evolution. The thick solid histogram represents the sum of all contributions. The KMR unintegrated parton densities in a proton are used.

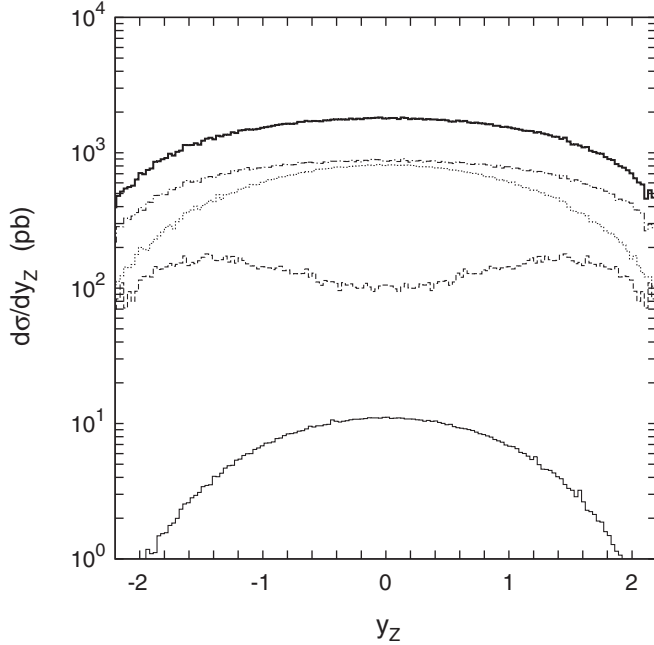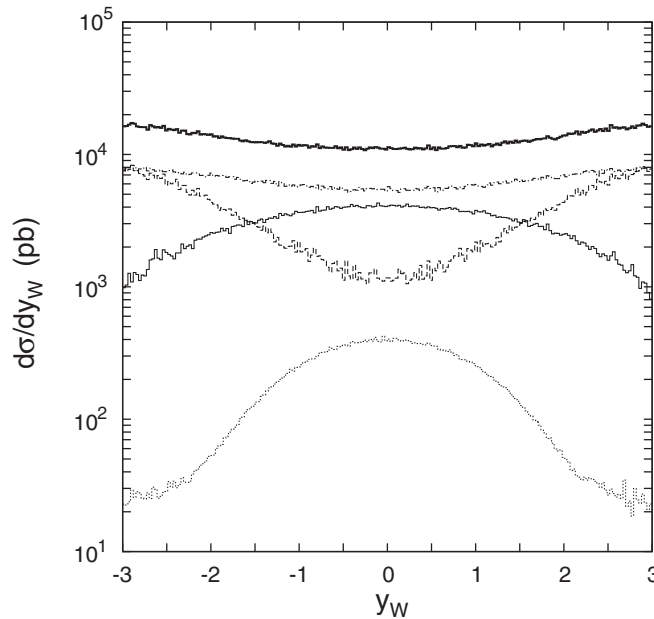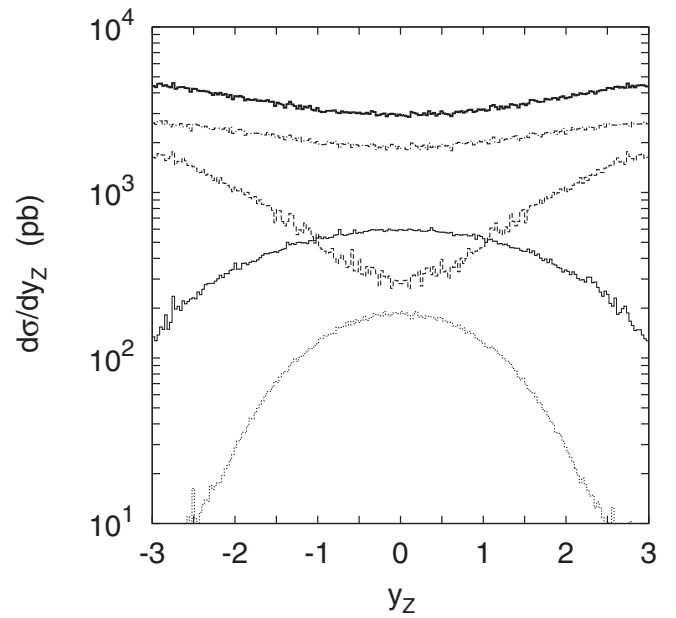[8]See, for example, review [29] for more details.

FIG. 4. Different contributions to the inclusive Z^0 boson production at the Tevatron conditions. Notations of histograms are the same as in Fig. 3.

over the valence contributions at the central rapidities. The contribution of the valence quark-antiquark annihilation subprocess is important at the Tevatron and gives only a few percents at the LHC energy. As expected, the contribution of the $q + g^* \to W^\pm/Z^0 + q'$ subprocess is significant in the forward rapidity region, $|y| > 2$. At this point,

FIG. 5. Different contributions to the inclusive $W^\pm$ boson production at the LHC conditions. Notations of histograms are the same as in Fig. 3.

FIG. 6. Different contributions to the inclusive Z^0 boson production at the LHC conditions. Notations of histograms are the same as in Fig. 3.

we can conclude that the gluon-gluon fusion becomes an important production mechanism at high energies and therefore should be taken into account in the calculations. However, we would like to note that there is an additional contribution which is not included in the simple decomposition scheme proposed above. As was mentioned above, in this scheme it was assumed that sea quarks appear only at the last gluon splitting and there is no contribution from the quarks coming from the earlier steps of the evolution (and we absorb the last step of the gluon ladder into the hard matrix element $g^* + g^* \to W^\pm/Z^0 + q + \bar{q}'$). It is not clear in advance whether the last gluon splitting dominates or not. In order to model this additional component, we have repeated the calculations using the KMR unintegrated quark densities (20) and the quark-antiquark annihilation $q + \bar{q}' \to W^\pm/Z^0$ matrix element. But in these evaluations we omitted the last term and keep only the sea quark in the first term of (20). Thus, we switch off the pure gluon component of the sea quark distributions and remove the valence quarks from the evolution ladder. In this way only the contributions to the $f_q(x, \mathbf{k}_T^2, \mu^2)$ originating from the earlier (involving quarks) evolution steps are taken into account. So, the dash-dotted histograms in Figs. 3–6 represent the results of our calculations. We have found the significant (by about of 50%) enhancement of the cross sections at both the Tevatron and LHC conditions. Therefore in all calculations below we will consider this mechanism as an additional production one. Finally, taking into account all described above components, we can conclude that the gluon-gluon fusion contributes about $\sim 1\%$ to the total cross section at the Tevatron and up to $\sim 25\%$ at LHC energies.
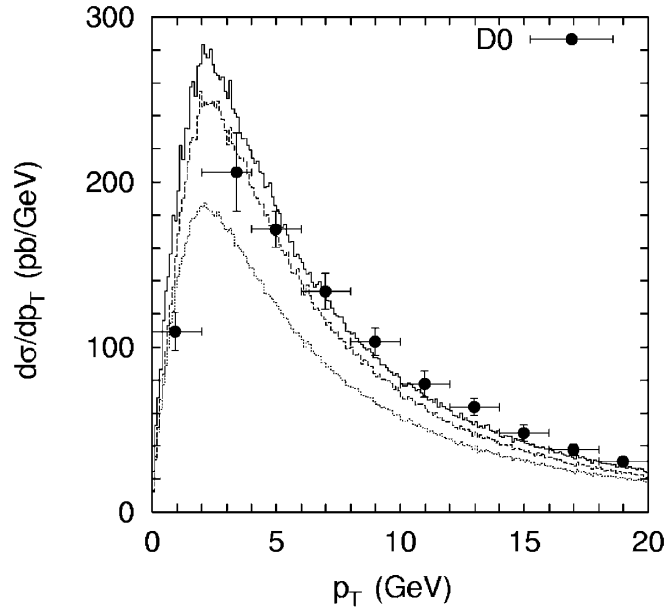
FIG. 7. Transverse momentum distribution of the $W^{\pm}$ boson production. The solid and dashed histograms correspond to the results obtained with the CCFM and KMR unintegrated gluon densities in a proton, respectively. The dotted histograms were obtained by using the quark-antiquark annihilation matrix element convoluted with the KMR unintegrated quark distributions. The cross sections times branching fraction $f(W \rightarrow l\nu)$ are shown. The experimental data are from D0 [9].

Now we turn to the transverse momentum distributions of the $W^{\pm}$ and Z^0 bosons. The experimental data for the transverse momentum distributions come from both the D0
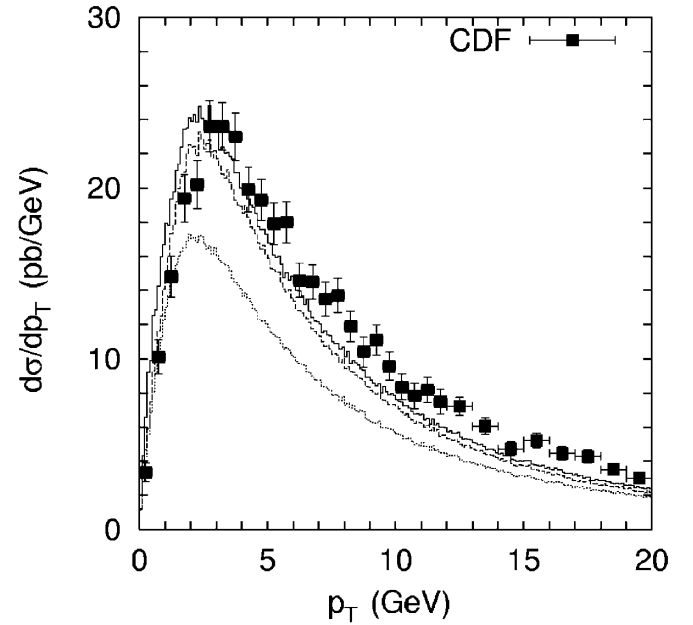
FIG. 9. Transverse momentum distribution of the Z^0 boson production. Notations of histograms are the same as in Fig. 7. The cross sections times branching fraction $f(Z \rightarrow l^+l^-)$ are shown. The experimental data are from CDF [4].

[8,9] and CDF [4] collaborations at the Tevatron. These data were obtained at the center-of-mass energy $\sqrt{s} = 1800$ GeV. Measurements were made for $W \rightarrow l\nu$ and $Z \rightarrow l^+l^-$ decays, so that we should multiply our theoretical predictions by the relevant branching fractions $f(W \rightarrow l\nu)$ and $f(Z \rightarrow l^+l^-)$. These branching fractions were set
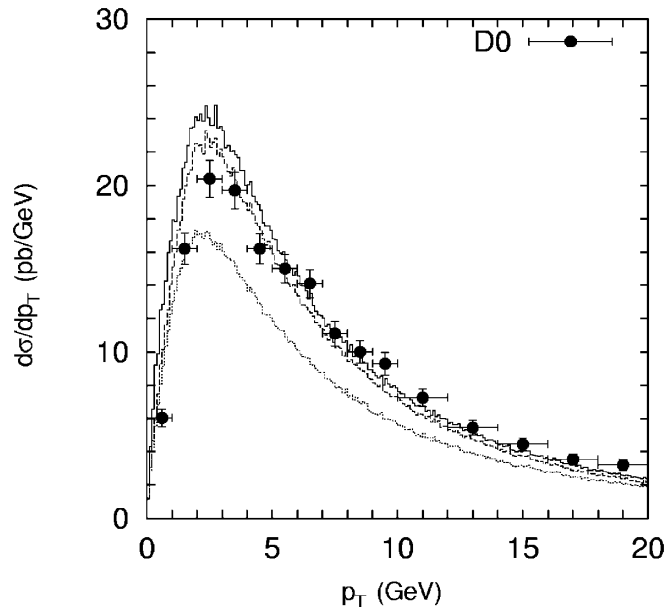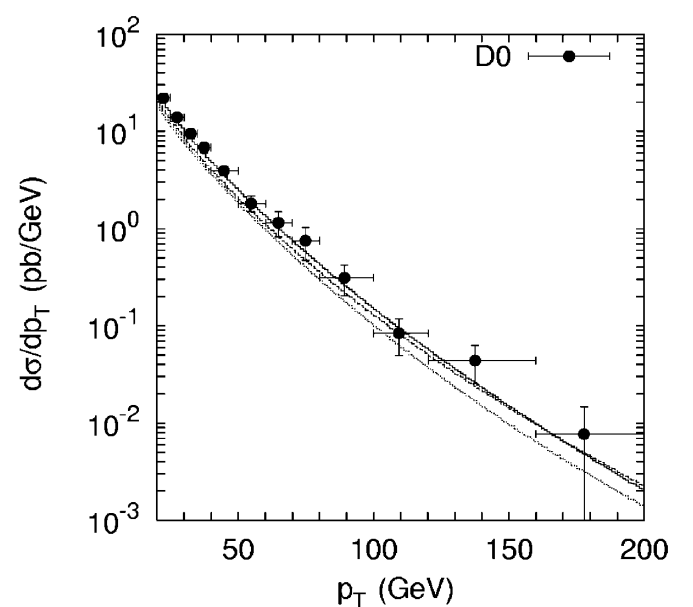

FIG. 8. Transverse momentum distribution of the Z^0 boson production. Notations of histograms are the same as in Fig. 7. The cross sections times branching fraction $f(Z \rightarrow l^+l^-)$ are shown. The experimental data are from D0 [8].

FIG. 10. Transverse momentum distribution of the $W^{\pm}$ boson production. Notations of histograms are the same as in Fig. 7. The cross sections times branching fraction $f(W \rightarrow l\nu)$ are shown. The experimental data are from D0 [9].
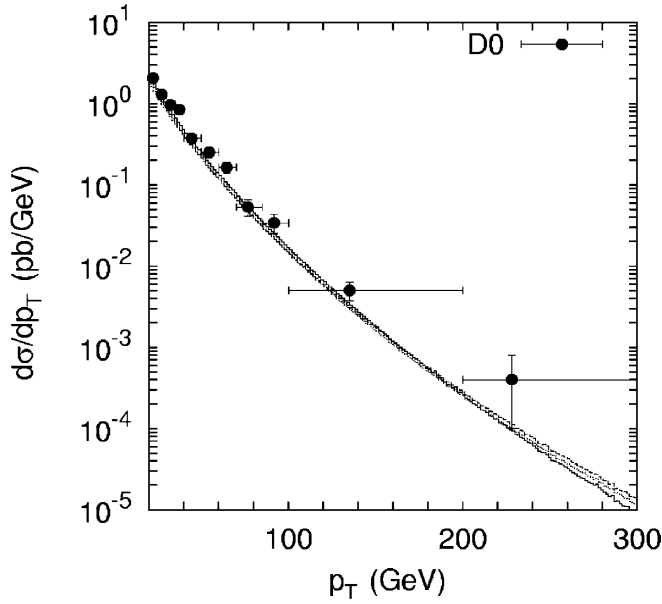
FIG. 11.   Transverse momentum distribution of the Z^0 boson production. Notations of histograms are the same as in Fig. 7. The cross sections times branching fraction $f(Z \to l^+ l^-)$ are shown. The experimental data are from D0 [8].

to $f(W \to l\nu) = 0.1075$ and $f(Z \to l^+ l^-) = 0.033\,66$ [40]. In Figs. 7–9 we display a comparison of the calculated differential cross sections $d\sigma/dp_T$ of the $W^\pm$ and Z^0 boson production with the experimental data [4,8,9] in the low p_T region, namely $p_T < 20$ GeV. Next, in Figs. 10–12, we demonstrate the $W^\pm$ and Z^0 transverse momentum
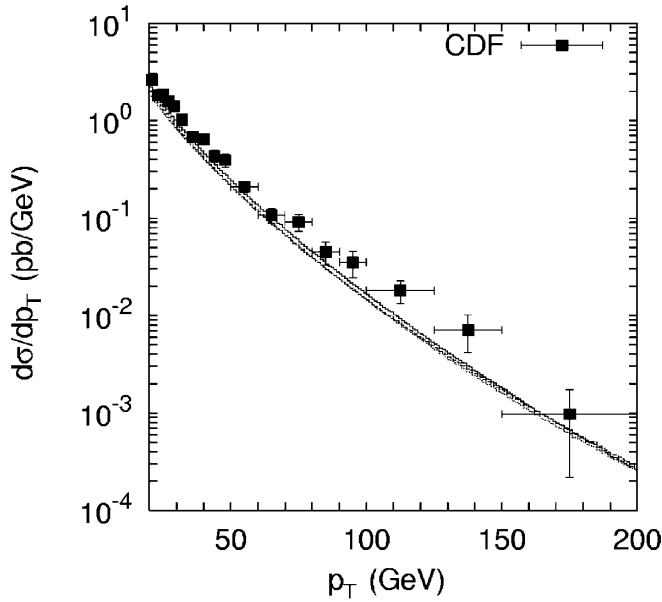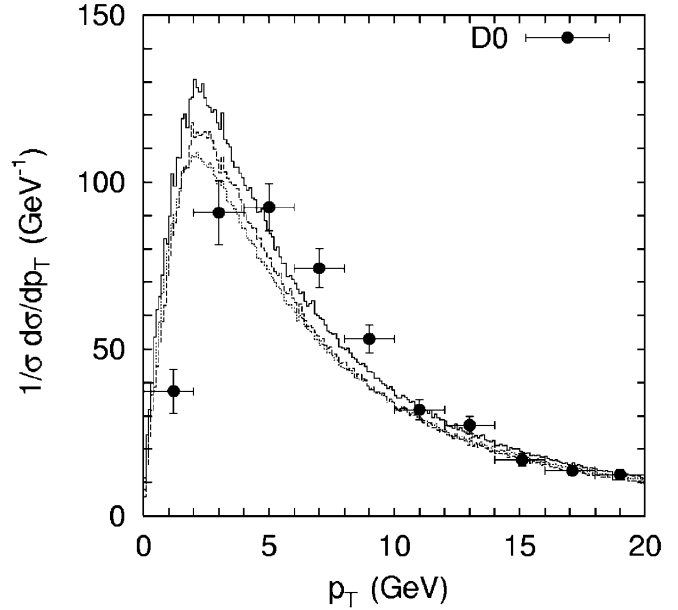

FIG. 13.   Normalized transverse momentum distribution of the $W^\pm$ boson production. Notations of histograms are the same as in Fig. 7. The earlier experimental data are from D0 [5].

distributions in the intermediate and high p_T regions. Additionally, in Figs. 13 and 14, we plot the normalized differential cross section $(1/\sigma)d\sigma/dp_T$ of the $W^\pm$ boson production. The solid and dashed histograms correspond to the results obtained with the CCFM and KMR unintegrated gluon densities, respectively. All contributions discussed above are taken into account. The dotted histograms were obtained using the quark-antiquark annihilation matrix

FIG. 12.   Transverse momentum distribution of the Z^0 boson production. Notations of histograms are the same as in Fig. 7. The cross sections times branching fraction $f(Z \to l^+ l^-)$ are shown. The experimental data are from CDF [4].
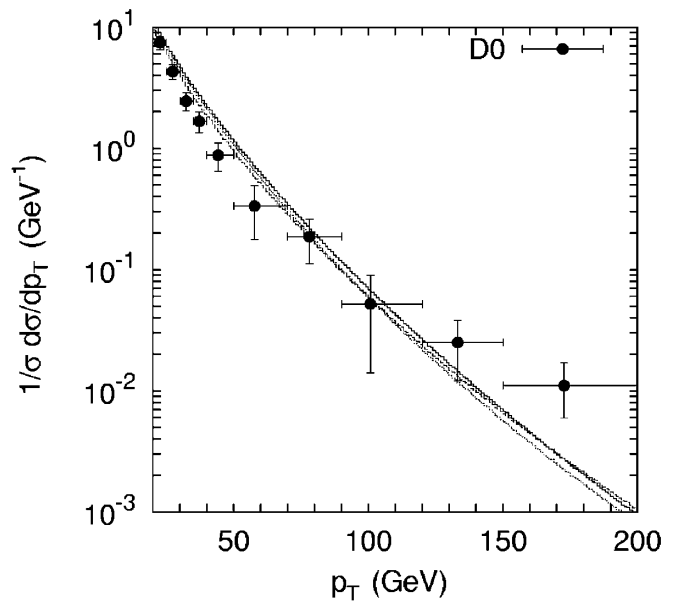

FIG. 14.   Normalized transverse momentum distribution of the $W^\pm$ boson production. Notations of histograms are the same as in Fig. 7. The earlier experimental data are from D0 [5].
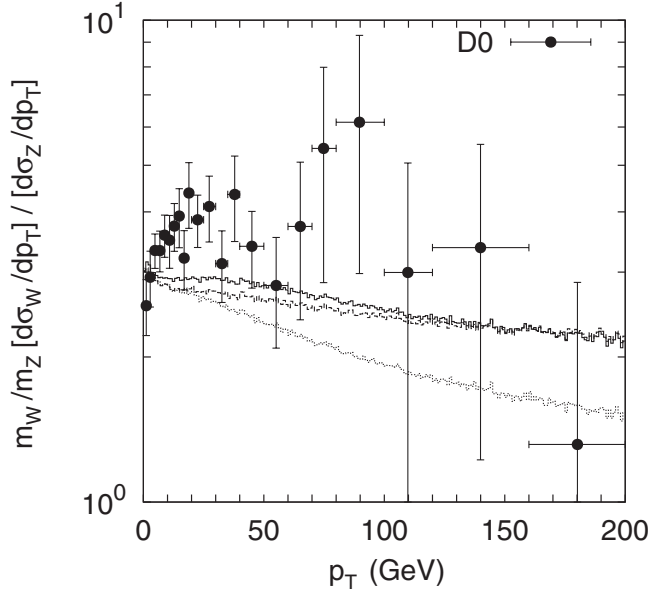
FIG. 15.   Ratio of the differential cross section for $W^{\pm}$ to Z^0 production. Notations of histograms are the same as in Fig. 7. The experimental data are from D0 [8].

element convoluted with the KMR unintegrated quark distributions in a proton (in this case the transverse momentum of the produced vector boson is defined by the transverse momenta of the incoming quarks). We found an increase in the cross section calculated in the proposed decomposition scheme (where only the unintegrated gluon densities were used). In this scheme, we obtain that both the CCFM and KMR gluon distributions reproduce well the Tevatron data within the uncertainties, although the KMR gluon tends to slightly underestimate the data in the low p_T region. The difference between the solid and dashed histograms in Figs. 7–14 is due to different behavior of the CCFM and KMR gluon densities. The predictions based of the quark-antiquark annihilation subprocess lie below the experimental data but agree with them in shape. This observation coincides with the one from [30] where an additional factor of about 1.2 was introduced to eliminate the visible disagreement between the data and theory.[9]

An additional possibility to distinguish the two calculation schemes comes from the studying of the ratio of the $W^{\pm}$ and Z^0 boson cross sections. In fact, since $W^{\pm}$ and Z^0 production properties are very similar, as the transverse momentum of the vector boson becomes smaller, the radiative corrections affecting the individual distributions and the cross sections of the hard process are factorized and canceled in this ratio. Therefore the results of the

[9]In Ref. [30] authors have explained the origin of this extra factor by the fact that the input parton densities (used to determine the unintegrated ones) should themselves be determined from data using the appropriate noncollinear formalism.
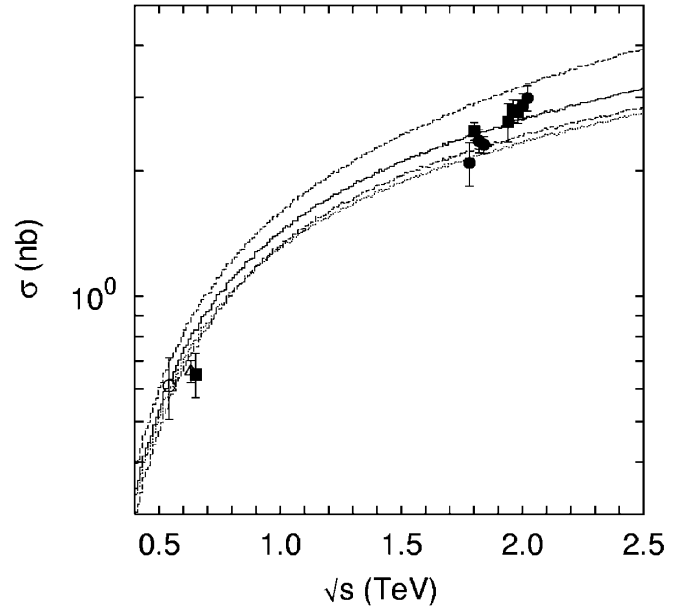

FIG. 16.   The total cross section of the inclusive $W^{\pm}$ boson production as a function of $\sqrt{s}$. The solid and dotted histograms correspond to the results obtained with the CCFM and KMR unintegrated gluon densities, respectively. The upper and lower dashed histograms correspond to the scale variations in the CCFM gluon density as it was described in the text. The cross sections times branching fraction $f(W \to l\nu)$ are shown. The experimental data are from UA1 [1], UA2 [2], D0 [6,7], and CDF [3].
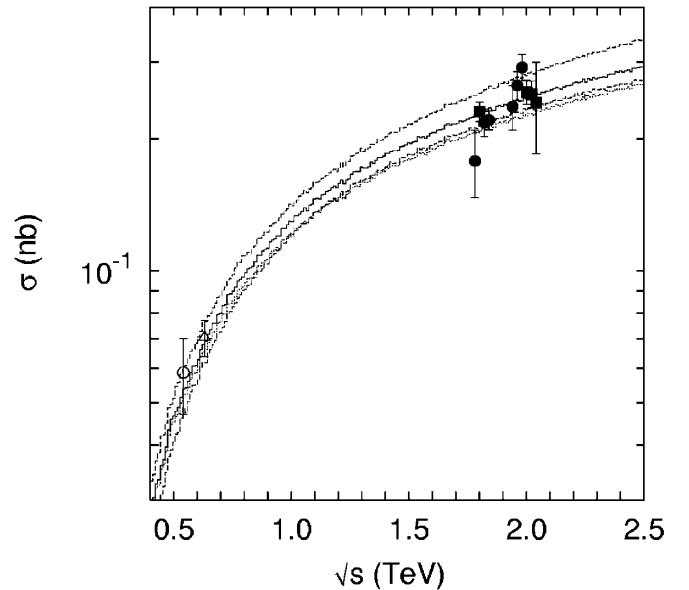

FIG. 17.   The total cross section of the inclusive Z^0 boson production as a function of $\sqrt{s}$. Notations of histograms are the same as in Fig. 16. The cross sections times branching fraction $f(Z \to l^+ l^-)$ are shown. The experimental data are from UA1 [1], UA2 [2], D0 [6,7], and CDF [3].

calculation of this ratio in the decomposition scheme (where the $\mathcal{O}(\alpha\alpha_s)$ and $\mathcal{O}(\alpha\alpha_s^2)$ subprocesses are taken into account) and the predictions based on the $\mathcal{O}(\alpha)$ quark-antiquark annihilation should differ from each other at moderate and high p_T values. This fact is clearly illustrated in Fig. 15 where the ratio of $W^{\pm}$ and Z^0 cross sections as a function of the transverse momentum is displayed. As was expected, there is practically no difference between all plotted histograms in the low p_T region.

As a final point of our study, we discuss the scale dependence of our results. In Figs. 16 and 17 we show the total cross section of the $W^{\pm}$ and Z^0 boson production as a function of the total center-of-mass energy $\sqrt{s}$. Here, the solid and dotted histograms correspond to the results obtained with the CCFM and KMR unintegrated gluon densities, respectively. The upper and lower dashed histograms correspond to the scale variations in the CCFM gluon density as it was described above. We find that the scale uncertainties are the same order approximately as the uncertainties coming from the unintegrated gluon distributions. This fact is the typical one for the leading-order k_T-factorization calculations. Our predictions for the $W^{\pm}$ and Z^0 boson total cross section agree well with the data in a wide $\sqrt{s}$ range.

IV. CONCLUSIONS

We have studied the production of electroweak gauge bosons in hadronic collisions at high energies in the k_T-factorization approach of QCD. Our consideration is based on the scheme which provides solid theoretical grounds for adequately taking into account the effects of initial parton momentum. The central part of our derivation is the off-shell gluon-gluon fusion subprocess $g^* + g^* \rightarrow W^{\pm}/Z^0 + q + \bar{q}'$. At the price of considering the corresponding matrix element rather than the $q + \bar{q}' \rightarrow W^{\pm}/Z^0$ one, we have reduced the problem of unknown unintegrated quark distributions to the problem of gluon distributions. This way enables us with making comparisons between the different parton evolution schemes and parametrizations of parton densities. Since the gluons are only responsible for the appearance of the sea, but not the valence quarks, the contribution from the valence quarks has been calculated separately. Having in mind that the valence quarks are only important at large x, where the traditional DGLAP evolution is accurate and reliable, we have calculated this contribution within the usual collinear scheme based on $q + g^* \rightarrow W^{\pm}/Z^0 + q'$ and $q + \bar{q}' \rightarrow W^{\pm}/Z^0$ partonic subprocesses and on-shell parton densities.

We have studied in detail the different production mechanisms of $W^{\pm}$ and Z^0 bosons. We find that the off-shell gluon-gluon fusion gives $\sim 1\%$ and $\sim 25\%$ contributions to the inclusive $W^{\pm}/Z^0$ production cross sections at the Tevatron and LHC. Specially we simulate the contri-

bution from the quarks involved into the earlier steps of the evolution cascade (i.e., into the second-to-last, third-to-last, and other gluon splittings) and find that these quarks play an important role at both the Tevatron and LHC energies. It was demonstrated that corresponding corrections should be taken into account in the numerical calculations within the k_T-factorization approach.

We have calculated the total and differential $W^{\pm}$ and Z^0 production cross sections and have made comparisons with the Tevatron data. In the numerical analysis we have used the unintegrated gluon densities obtained from the CCFM evolution equation and from the KMR prescription. Our numerical results agree well with the experimental data.

When the present paper was ready for publication, we have learned about the results obtained by M. Deak and F. Schwennsen [41], who used the same theoretical approach, but focused attention on slightly different aspects of the problem. These authors concentrate on the associated $W^{\pm}/Z^0$ production with heavy quark pairs (mainly on the $Zb\bar{b}$ final state), where the gluon-gluon fusion subprocess dominates. In additional to that, we consider quark subprocesses, which are important for inclusive $W^{\pm}/Z^0$ production. We show that the experimental data can be described with taking quark contributions into account.

APPENDIX: A

Here we present the compact analytic expressions for the cross section of the $W^{\pm}/Z^0$ production via the $q + \bar{q}' \rightarrow W^{\pm}/Z^0$ subprocess in the k_T-factorization approach. Let us define the transverse momenta and azimuthal angles of the incoming quark q and antiquark $\bar{q}'$ as $\mathbf{k}_{1T}$ and $\mathbf{k}_{2T}$ and ϕ_1 and ϕ_2, respectively. The produced vector boson has the transverse momentum $\mathbf{p}_T$ ($\mathbf{p}_T = \mathbf{k}_{1T} + \mathbf{k}_{2T}$) and center-of-mass rapidity y. The $W^{\pm}/Z^0$ production cross section can be written as

$$\sigma(p + \bar{p} \to W^{\pm}/Z^0 + X) = \sum_q \int \frac{2\pi}{(x_1 x_2 s)^2} |\bar{\mathcal{M}}(q + \bar{q}' \to W^{\pm}/Z^0)|^2$$

$$\times f_q(x_1, \mathbf{k}_{1T}^2, \mu^2) f_q(x_2, \mathbf{k}_{2T}^2, \mu^2) d\mathbf{k}_{1T}^2 d\mathbf{k}_{2T}^2 dy \frac{d\phi_1}{2\pi} \frac{d\phi_2}{2\pi}, \tag{A1}$$

where $f_q(x, \mathbf{k}_T^2, \mu^2)$ is the unintegrated quark distributions given by (20). In the high-energy limit the fractions x_1 and x_2 of the initial proton's longitudinal momenta are given by

$$x_1\sqrt{s} = m_T e^y, \qquad x_2\sqrt{s} = m_T e^{-y}, \tag{A2}$$

where m_T is the transverse mass of the vector boson. The squared matrix element $|\bar{\mathcal{M}}(q + \bar{q}' \to W^{\pm})|^2$ summed over final polarization states and averaged over initial ones is

$$|\bar{\mathcal{M}}(q + \bar{q}' \to W^{\pm})|^2$$

$$= -\frac{e^2}{72 m_W^2 \sin^2\theta_W}[(m_1^2 - m_2^2)^2 + m_W^2(m_1^2 + m_2^2) - 2m_W^4], \tag{A3}$$

where m_1 and m_2 are the masses of incoming quarks. In the case of Z^0 boson production, the squared matrix element $|\bar{\mathcal{M}}(q + \bar{q} \to Z^0)|^2$ summed over final polarization states and averaged over initial ones is

$$|\bar{\mathcal{M}}(q + \bar{q} \to Z^0)|^2$$

$$= \frac{2e^2}{9\sin^2 2\theta_W} \times [(m_Z^2 - m^2)[I_3^{(q)}]^2 + 2e_q(2m^2 + m_Z^2)$$

$$\times \sin^2\theta_W(e_q\sin^2\theta_W - I_3^{(q)})], \tag{A4}$$

where m, e_q, and $I_3^{(q)}$ are the mass, fractional electric charge, and weak isospin of the incoming quark. Note that there is no obvious dependence on the transverse momenta of the initial quark and antiquark. However, this dependence is present because the true off-shell kinematics is used. In particular, the incident parton momentum fractions x_1 and x_2 have some $\mathbf{k}_T$ dependence. If we take the limit $\mathbf{k}_{1T}^2 \to 0$ and $\mathbf{k}_{2T}^2 \to 0$, then we recover the relevant expression in the standard collinear approximation of QCD.

APPENDIX: B

Here we present the analytic expressions for the cross section of the $W^{\pm}/Z^0$ production via the $q + g^* \to W^{\pm}/Z^0 + q'$ subprocess in the k_T-factorization approach. Let us define the transverse momenta and azimuthal angles of the incoming quark and off-shell gluon as $\mathbf{k}_{1T}$ and $\mathbf{k}_{2T}$ and ϕ_1 and ϕ_2, respectively. In the following, $\hat{s}$, $\hat{t}$, and $\hat{u}$ are usual Mandelstam variables for the $2 \to 2$ subprocess. The $W^{\pm}/Z^0$ production cross section can be written as follows:

$$\sigma(p + \bar{p} \to W^{\pm}/Z^0 + X) = \sum_q \int \frac{1}{16\pi(x_1 x_2 s)^2} |\bar{\mathcal{M}}(q + g^* \to W^{\pm}/Z^0 + q')|^2$$

$$\times f_q(x_1, \mathbf{k}_{1T}^2, \mu^2) f_g(x_2, \mathbf{k}_{2T}^2, \mu^2) d\mathbf{k}_{1T}^2 d\mathbf{k}_{2T}^2 d\mathbf{p}_T^2 dy dy' \frac{d\phi_1}{2\pi} \frac{d\phi_2}{2\pi}, \tag{B1}$$

where y' is the rapidity of the final quark q'. The fractions x_1 and x_2 of the initial proton's longitudinal momenta are given by

$$x_1\sqrt{s} = m_T e^y + m_T' e^{y'}, \qquad x_2\sqrt{s} = m_T e^{-y} + m_T' e^{-y'}, \tag{B2}$$

where m_T and m_T' are the transverse masses of the vector

boson and final quark q'. If we take the limit $\mathbf{k}_{1T}^2 \to 0$ and $\mathbf{k}_{2T}^2 \to 0$, then we recover the relevant expression in the usual collinear approximation. The squared matrix elements $|\bar{\mathcal{M}}(q + g^* \to W^{\pm} + q')|^2$ and $|\bar{\mathcal{M}}(q + g^* \to Z^0 + q)|^2$ summed over final polarization states and averaged over initial ones are

$$|\bar{\mathcal{M}}(q + g^* \to W^{\pm} + q')|^2 = \frac{e^2 g^2}{192\sin^2\theta_W} \frac{F_W}{(m_1^2 - \hat{s})^2(m_2^2 - \hat{t})^2 m_W^2}, \tag{B3}$$

$$|\bar{\mathcal{M}}(q + g^* \to Z^0 + q)|^2 = \frac{2e^2 g^2}{3\sin^2 2\theta_W} \frac{F_Z}{(m^2 - \hat{s})^2(m^2 - \hat{t})^2 m_Z^2}, \tag{B4}$$

where

$$
\begin{aligned}
F_W = {} & -8(m_1^8(3m_2^2 - \hat{t}) + m_1^6(m_2^4 + m_2^2(2m_W^2 - 5\hat{s} - 7\hat{t}) + \hat{t}(\hat{s} + 2\hat{t})) + m_1^4(m_2^6 + m_2^4(8m_W^2 - 3(\hat{s} + \hat{t})) \\
& + m_2^2(-6m_W^4 + 3\hat{s}^2 + 13\hat{s}\,\hat{t} + 5\hat{t}^2 - 6m_W^2(\hat{s} + \hat{t})) - \hat{t}(-2m_W^4 - 2m_W^2\hat{s} + (\hat{s} + \hat{t})^2)) \\
& + m_1^2(3m_2^8 + m_2^6(2m_W^2 - 7\hat{s} - 5\hat{t}) + m_2^4(-6m_W^4 + 5\hat{s}^2 + 13\hat{s}\,\hat{t} + 3\hat{t}^2 - 6m_W^2(\hat{s} + \hat{t})) \\
& + m_2^2(4m_W^6 - \hat{s}^3 - 11\hat{s}^2\hat{t} - 11\hat{s}\hat{t}^2 - \hat{t}^3 \\[4pt]
& + 6m_W^4(\hat{s} + \hat{t}) + 6m_W^2(\hat{s}^2 + \hat{t}^2)) + \hat{t}(-4m_W^6 + 2m_W^4\hat{s} + \hat{s}(\hat{s} + \hat{t})^2 - 2m_W^2(2\hat{s}^2 - \hat{s}\,\hat{t} + \hat{t}^2))) \\
& + \hat{s}(-m_2^8 + m_2^6(2\hat{s} + \hat{t}) + 2m_W^2\hat{t}(2m_W^4 + \hat{s}^2 + \hat{t}^2 - 2m_W^2(\hat{s} + \hat{t})) + m_2^4(2m_W^4 + 2m_W^2\hat{t} - (\hat{s} + \hat{t})^2) \\
& + m_2^2(-4m_W^6 + 2m_W^4\hat{t} + \hat{t}(\hat{s} + \hat{t})^2 - 2m_W^2(\hat{s}^2 - \hat{s}\,\hat{t} + 2\hat{t}^2))) + (m_1^8 + m_2^8 + m_1^6(m_W^2 - 2(\hat{s} + \hat{t})) \\
& + m_2^6(m_W^2 - 2(\hat{s} + \hat{t})) \\[4pt]
& + m_2^4(-2m_W^4 - 2m_W^2\hat{t} + (\hat{s} + \hat{t})^2) + m_2^2m_W^2(5\hat{s}^2 + 4\hat{s}\,\hat{t} + \hat{t}^2 + m_W^2(-8\hat{s} + 4\hat{t})) \\
& - 2m_W^2(2\hat{s}\,\hat{t}(\hat{s} + \hat{t}) + m_W^2(\hat{s}^2 - 4\hat{s}\,\hat{t} + \hat{t}^2)) + m_1^4(-2m_2^2 - 2m_W^4 - 2m_W^2\hat{s} + (\hat{s} + \hat{t})^2 + m_2^2(m_W^2 + 2(\hat{s} + \hat{t}))) \\
& + m_1^2(m_W^2(\hat{s}^2 + 4m_W^2(\hat{s} - 2\hat{t}) + 4\hat{s}\,\hat{t} + 5\hat{t}^2) + m_2^4(m_W^2 + 2(\hat{s} + \hat{t})) \\
& + m_2^2(8m_W^4 - 6m_W^2(\hat{s} + \hat{t}) - 2(\hat{s} + \hat{t})^2)))(-\mathbf{k}_{2T}^2) + 4m_W^2(m_1^2 - \hat{s})(m_2^2 - \hat{t})\mathbf{k}_{2T}^4,
\end{aligned}
$$

$$
\begin{aligned}
F_Z = {} & -2e_q I_3^{(q)} m_Z^2 \sin^2\theta_W(6m^8 - \hat{s}\,\hat{t}(2m_Z^4 + \hat{s}^2 + \hat{t}^2 - 2m_Z^2(\hat{s} + \hat{t})) - m^4(2m_Z^4 + 3\hat{s}^2 + 14\hat{s}\,\hat{t} + 3\hat{t}^2 - 2m_Z^2(\hat{s} + \hat{t})) \\
& + m^2(\hat{s}^3 - 8m_Z^2\hat{s}\,\hat{t} + 7\hat{s}^2\hat{t} + 7\hat{s}\hat{t}^2 + \hat{t}^3 + 2m_Z^4(\hat{s} + \hat{t}))) + 2e_q^2 m_Z^2 \sin^4\theta_W(6m^8 - \hat{s}\,\hat{t}(2m_Z^4 + \hat{s}^2 + \hat{t}^2 - 2m_Z^2(\hat{s} + \hat{t})) \\
& - m^4(2m_Z^4 + 3\hat{s}^2 + 14\hat{s}\,\hat{t} + 3\hat{t}^2 - 2m_Z^2(\hat{s} + \hat{t})) + m^2(\hat{s}^3 - 8m_Z^2\hat{s}\,\hat{t} + 7\hat{s}^2\hat{t} + 7\hat{s}\hat{t}^2 + \hat{t}^3 \\[4pt]
& + 2m_Z^4(\hat{s} + \hat{t}))) + [I_3^{(q)}]^2(-4m^{10} + m^8(-6m_Z^2 + 8(\hat{s} + \hat{t})) - m_Z^2\hat{s}\,\hat{t}(2m_Z^4 + \hat{s}^2 + \hat{t}^2 - 2m_Z^2(\hat{s} + \hat{t})) \\
& + m^6(6m_Z^4 - 5\hat{s}^2 - 14\hat{s}\,\hat{t} - 5\hat{t}^2 + 6m_Z^2(\hat{s} + \hat{t})) + m^4(-2m_Z^6 + \hat{s}^3 + 7\hat{s}^2\hat{t} + 7\hat{s}\hat{t}^2 + \hat{t}^3 - 4m_Z^4(\hat{s} + \hat{t}) \\
& - m_Z^2(3\hat{s}^2 + 2\hat{s}\,\hat{t} + 3\hat{t}^2)) + m^2(-2m_Z^4\hat{s}\,\hat{t} + 2m_Z^6(\hat{s} + \hat{t}) - \hat{s}\,\hat{t}(\hat{s} + \hat{t})^2 + m_Z^2(\hat{s}^3 + \hat{s}^2\hat{t} + \hat{s}\hat{t}^2 + \hat{t}^3))) \\[4pt]
& + m_Z^2(2e_q I_3^{(q)} \sin^2\theta_W(2m^4(m_Z^2 - \hat{s} - \hat{t}) - 2\hat{s}\,\hat{t}(\hat{s} + \hat{t}) - m_Z^2(\hat{s}^2 - 4\hat{s}\,\hat{t} + \hat{t}^2) - 2m^2(-4\hat{s}\,\hat{t} + m_Z^2(\hat{s} + \hat{t}))) \\
& + 2e_q^2 \sin^4\theta_W(2\hat{s}\,\hat{t}(\hat{s} + \hat{t}) + 2m^4(-m_Z^2 + \hat{s} + \hat{t}) + m_Z^2(\hat{s}^2 - 4\hat{s}\,\hat{t} + \hat{t}^2) + 2m^2(-4\hat{s}\,\hat{t} + m_Z^2(\hat{s} + \hat{t}))) \\
& + [I_3^{(q)}]^2(-2m^6 + 2\hat{s}\,\hat{t}(\hat{s} + \hat{t}) \\
& + m_Z^2(\hat{s}^2 - 4\hat{s}\,\hat{t} + \hat{t}^2) + m^4(-2m_Z^2 + 4(\hat{s} + \hat{t})) + m^2(-3\hat{s}^2 - 4\hat{s}\,\hat{t} - 3\hat{t}^2 + 2m_Z^2(\hat{s} + \hat{t}))))(-\mathbf{k}_{2T}^2) \\
& - 2m_Z^2(m^2 - \hat{s})([I_3^{(q)}]^2 - 2e_q I_3^{(q)} \sin^2\theta_W + 2e_q^2 \sin^4\theta_W)(m^2 - \hat{t})\mathbf{k}_{2T}^4.
\end{aligned}
\tag{B5}
$$

[1] C. Albajar *et al.* (UA1 Collaboration), Phys. Lett. B **253**, 503 (1991).

[2] J. Alitti *et al.* (UA2 Collaboration), Z. Phys. **47**, 11 (1990).

[3] F. Abe *et al.* (CDF Collaboration), Phys. Rev. Lett. **76**, 3070 (1996).

[4] B. Affolder *et al.* (CDF Collaboration), Phys. Rev. Lett. **84**, 845 (2000).

[5] B. Abbott *et al.* (D0 Collaboration), Phys. Rev. Lett. **80**, 5498 (1998).

[6] S. Abachi *et al.* (D0 Collaboration), Phys. Rev. Lett. **75**, 1456 (1995).

[7] B. Abbott *et al.* (D0 Collaboration), Phys. Rev. D **61**, 072001 (2000).

[8] B. Abbott *et al.* (D0 Collaboration), Phys. Rev. D **61**, 032004 (2000).

[9] B. Abbott *et al.* (D0 Collaboration), Phys. Lett. B **513**, 292 (2001).

[10] P. Sutton, A. Martin, R. Roberts, and W. J. Stirling, Phys. Rev. D **45**, 2349 (1992).

[11] R. Rijken and W. van Neerven, Phys. Rev. D **51**, 44 (1995).

[12] R. Hamberg, W. van Neerven, and T. Matsuura, Nucl. Phys. **B359**, 343 (1991).

[13] R. Harlander and W. Kilgore, Phys. Rev. Lett. **88**, 201801 (2002).

[14] W. van Neerven and E. Zijstra, Nucl. Phys. **B382**, 11 (1992).

[15] J. Collins, D. Soper, and G. Sterman, Nucl. Phys. **B250**, 199 (1985); J. Collins and D. Soper, Nucl. Phys. **B193**, 381 (1981); **B197**, 446 (1982).

[16] C. Davies, B. Webber, and W. J. Stirling, Nucl. Phys. **B256**, 413 (1985); C. Davies and W. J. Stirling, Nucl. Phys. **B244**, 337 (1984).

[17] G. Altarelli, R. K. Ellis, M. Grego, and G. Martinelli, Nucl. Phys. **B246**, 12 (1984).

[18] P. B. Arnold and R. Kauffman, Nucl. Phys. **B349**, 381 (1991).

[19] G. A. Ladinsky and C. P. Yuan, Phys. Rev. D **50**, R4239 (1994).

[20] R. K. Ellis and S. Veseli, Nucl. Phys. **B511**, 649 (1998).

[21] C. Balazs and C. P. Yuan, Phys. Rev. D **56**, 5558 (1997).

[22] A. Kulesza and W. J. Stirling, Nucl. Phys. **B555**, 279 (1999).

[23] L. V. Gribov, E. M. Levin, and M. G. Ryskin, Phys. Rep. **100**, 1 (1983); E. M. Levin, M. G. Ryskin, Yu. M. Shabelsky, and A. G. Shuvaev, Sov. J. Nucl. Phys. **53**, 657 (1991).

[24] S. Catani, M. Ciafoloni, and F. Hautmann, Nucl. Phys. **B366**, 135 (1991); J. C. Collins and R. K. Ellis, Nucl. Phys. **B360**, 3 (1991).

[25] E. A. Kuraev, L. N. Lipatov, and V. S. Fadin, Sov. Phys. JETP **44**, 443 (1976); **45**, 199 (1977); I. I. Balitsky and L. N. Lipatov, Sov. J. Nucl. Phys. **28**, 822 (1978).

[26] M. Ciafaloni, Nucl. Phys. **B296**, 49 (1988); S. Catani, F. Fiorani, and G. Marchesini, Phys. Lett. B **234**, 339 (1990); Nucl. Phys. **B336**, 18 (1990); G. Marchesini, Nucl. Phys. **B445**, 49 (1995).

[27] V. N. Gribov and L. N. Lipatov, Yad. Fiz. **15**, 781 (1972); L. N. Lipatov, Sov. J. Nucl. Phys. **20**, 94 (1975); G. Altarelli and G. Parisi, Nucl. Phys. **B126**, 298 (1977); Y. L. Dokshitzer, Sov. Phys. JETP **46**, 641 (1977).

[28] A. Gawron and J. Kwiecinski, Phys. Rev. D **70**, 014003 (2004).

[29] B. Andersson *et al.* (Small-*x* Collaboration), Eur. Phys. J. C **25**, 77 (2002); J. Andersen *et al.* (Small-*x* Collaboration), Eur. Phys. J. C **35**, 67 (2004); **48**, 53 (2006).

[30] G. Watt, A. D. Martin, and M. G. Ryskin, Phys. Rev. D **70**, 014012 (2004).

[31] M. A. Kimber, A. D. Martin, and M. G. Ryskin, Phys. Rev. D **63**, 114027 (2001); G. Watt, A. D. Martin, and M. G. Ryskin, Eur. Phys. J. C **31**, 73 (2003).

[32] A. V. Bogdan and A. V. Grabovsky, Nucl. Phys. **B773**, 65 (2007).

[33] S. P. Baranov, A. V. Lipatov, and N. P. Zotov, Phys. Rev. D **77**, 074024 (2008).

[34] J. A. M. Vermaseren, *Symbolic Manipulation With FORM* (Computer Algebra Nederland, Kruislaan, SJ Amsterdaam, 1991), p. 413, ISBN 90-74116-01-9.

[35] R. E. Prange, Phys. Rev. **110**, 240 (1958); S. P. Baranov, Phys. At. Nucl. **60**, 1322 (1997).

[36] G. P. Lepage, J. Comput. Phys. **27**, 192 (1978).

[37] M. Glück, E. Reya, and A. Vogt, Phys. Rev. D **46**, 1973 (1992); Z. Phys. C **67**, 433 (1995).

[38] H. Jung, A. V. Kotikov, A. V. Lipatov, and N. P. Zotov, in Proceedings of ICHEP'06, p. 493 (unpublished).

[39] H. Jung, Mod. Phys. Lett. A **19**, 1 (2004).

[40] W.-M. Yao *et al.* (Particle Data Group), J. Phys. G **33**, 1 (2006).

[41] M. Deak and F. Schwennsen, arXiv:0805.3763.